www.czasopisma.pan.pl PAN www.journals.pan.pl
Opto-Electronics Review 27 (2019) 194–201

Contents lists available at ScienceDirect

Opto-Electronics Review

journal homepage: http://www.journals.elsevier.com/opto-electronics review

Optoelectronic pressure dependent study of $MgZrO_3$ oxide and ground state thermoelectric response using Ab-initio calculations

N.A. Noor [a], M. Rashid [b,*], Q. Mahmood [c], B. Ul Haq [d,e], M.A. Naeem [f], A. Laref [g]

[a] Center for High Energy Physics, University of the Punjab, Lahore, 54000, Pakistan
[b] COMSATS University Islamabad, 44000, Pakistan
[c] Institute of Physics, GC University, Lahore, 54000, Pakistan
[d] Advanced Functional Materials & Optoelectronics Laboratory (AFMOL), Department of Physics, Faculty of Science, King Khalid University, P.O. Box 9004, Abha, Saudi Arabia
[e] Research Center for Advanced Materials Science (RCAMS), King Khalid University, Abha 61413, P.O. Box 9004, Saudi Arabia
[f] Department of electrical engineering, University of Punjab, Lahore, 54000, Pakistan
[g] Department of Physics and Astronomy, College of Science, King Saud University, Riyadh, 11451, King, Saudi Arabia

ARTICLE INFO

Article history:
Received 18 April 2018
Received in revised form 3 October 2018
Accepted 22 October 2018

Keywords:
Pressure-induced structure
Direct band gap semiconductors
Thermal efficiency
Dispersion light
Density functional theory (DFT)

ABSTRACT

The electronic, optical and thermoelectric properties of zirconia-based $MgZrO_3$ oxide have been studied theoretically at a variant pressure up to 25 GPa. Calculations for the formation energy and tolerance factor reveal the thermodynamic and structural stability of $MgZrO_3$. To tune the indirect band gap from to a direct band gap, the optimized structure of $MgZrO_3$ has been subjected to external pressure up to 25 GPa. The optical properties have been discussed in the form of dielectric constant and refraction that brief us about the dispersion, polarization, absorption, and transparency of the $MgZrO_3$. In the end, the thermoelectric parameters have been analyzed at variant pressure against the chemical potential and temperature. The narrow band gap and high absorption in the ultraviolet region increase the demand of the studied oxide for energy harvesting device applications.

1. Introduction

The progress in modern technology gives birth to new integrated devices with promising commercial features [1]. These commercially produced features include miniaturization, high-speed functioning etc. are strongly dependent on the inherent properties of base materials. Thus, deeper understanding and manipulation of these inherent properties of the base materials are mandatory, which leads scientists to investigate and optimize material parameters exhibiting aspects of materials [2–4]. The inherent properties of materials are significantly governed by the crystallographic structure. However, the efficiency and performance of these materials are found to be vulnerable to change in the external pressure. For example, in literature perovskite materials ($MAPbI_3$ i.e; MA = methyl ammonium) are known for their illustration of structural diversity from cubic to orthorhombic transition at 2.7 GPa and beyond 4.7 GPa crystalline to amorphous nature phase transition have been reported [5]. Furthermore, optical band gap tuning of perovskite materials ($BiBO_3$ and $BiAlO_3$) with pressure have been systematically demonstrated by Noor *et al.* [6].

All these facts motivated scientists and researchers for optimization of material characteristic and for the search of novel materials. Further, it requires stabilizing some new phases, which don't exisit at ordinary conditions. The naturally unstable phases are stabilized by using non-equilibrium growth techniques. In order to reveal novel properties of cubic semiconductors, hexagonal Si and Ge structures have also been realized, stabilized, demonstrated, investigated and reported [7,8]. These materials which are stabilized in two different structural phases are promising for advanced technological applications and applications. Moreover, investigations show that for an unstable phase, surface stabilizing not only possible but also vice versa is true [9].

Our present investigation focuses on the comparatively less studied $MgZrO_3$ perovskite. This studied perovskite is widely known for thermal barrier coatings due to their low thermal expansion [10]. This perovskite $MgZrO_3$ material is also used as a base catalyst, because of their high activity and durability in order to produce an efficient biodiesel catalyst [11]. Cubic structure is very

* Corresponding author.
E-mail addresses: rapakistana@yahoo.com, muhammad.rashid@comsats.edu.pk (M. Rashid).

https://doi.org/10.1016/j.opelre.2018.10.002
1230-3402/

simple in nature and well investigated, because of these facts, they are considered almost perfect for device applications. The polarization effects tend to limit the capability and efficiency of optoelectronic device applications, this limitation is currently being investigated for $CaZrO_3$, $SrZrO_3$ and $BaZrO_3$ perovskites subdue this polarization effect [12–14]. Not only, these facts and reason but also less explored and investigated $MgZrO_3$ intrigued us to investigate the cubic phase for physical aspects like electronic structure, optical under pressure. The manipulation and tuning of the band gap magnitude and its specific nature motivated us to investigate their thermoelectric aspects under pressure as well.

2. Method of calculations

We investigate the physical properties by simulating the FP-LAPW + lo method at ground state, which operates under the density functional theory (DFT) [15]. This method solves Kohn-Sham equations [16] and reveals corresponding eigen values and eigen functions. Under pressure electronic, optical and thermoelectric aspects have been determined by considering the fourth order of generalized gradient approximation (GGA) functional of exchange-correlation potential devised by Perdew-Burke-Ernzerh of (PBEsol) [17]. The states of Mg, Zr and O, both valence and core states are considered to be self-consistent. These self-consistent states are respectively realized in relativistic and semi-relativistic approximation in a spherical approximation. These approximations do not include spin-orbit couplings. The plane wave basis set comprises of charge density, wave function and potential expansion within the spheres surrounded by the atomic sites provided that these spheres are non- overlapping and the interstitial region of the unit cell.

The Fourier expanded charge density G_{max} is considered 18 $(Ry)^{1/2}$ and maximum quantum number Imax is considered to 10 for the wave expansion in the atomic sphere. However, convergence parameters i.e $R_{MT} \times K_{max}$ is considered to be 8. Convergence parameters are used to limit the size of the basis set. The average muffin-tin sphere radius is represented by the R_{MT} and maximum modulus of the reciprocal lattice is represented by K_{max}. For Mg, Zr and O, the values of R_{MT} are as 1.96, 1.68 and 1.73 respectively in atomic units. The sample of the reciprocal space is produced by $10 \times 10 \times 10$ Monkhorste Pack mesh in the irreducible Brillouin zone (IBZ) with 84 k-points [18]. Every calculation uses repetitive iteration process until each calculation converges to the total energy of crystal to 10^{-5}Ry. The Classical transport theory based BoltzTrap code [19] was used to calculate the thermoelectric properties of the studied oxide. The relaxation time is employed to be continual in BoltzTrap code because it cannot originate from band structure calculations [19].

3. Results and discussion

3.1. The stability and electronic behavior

The stability of the structure is very important for the device fabrication. We have confirmed the stability of $MgZrO_3$ in cubic phase at different pressures by calculating formation energy and Goldschmidt's tolerance factor. The formation energy measures the energy released when individual elements combined to form compounds as shown from the equation $\Delta H_f = E_{Total}(Mg_lZr_mO_n) - lE_{Mg} - mE_{Zr} - nE_O$, here $E_{Total}(Mg_lZr_mO_n)$ is the total energy of $MgZrO_3$, E_{Mg}, E_{Zr} and E_O are the energies of the Mg, Zr and O elements [20,21]. The negative sign of energy released to represent the stability of the studied oxide as shown in Table 1. Furthermore, the stability of $MgZrO_3$ increases with increasing the pressure may be due to the removal of phonons from the structure as the band gap convert from indirect to direct which we discuss later. Moreover, the Goldschmidt tolerance factor has been calculated through the following relation, $t = (r_{Mg} + r_O)/\sqrt{2}(r_{Zr} + r_O)$, here r_{Mg}, r_{Zr} and r_O are ionic radii of cations and anions. The range of tolerance factor from 0.90 to 1.1 is considered best for stable compounds [22]. Therefore, the calculated tolerance factor of our studied oxide approaches 1 with rising pressure that shows the structural symmetry increases by shifting the electronic states because of reasons explained above.

Table 1
Calculated lattice constant a(Å), bulk moduli B(GPa), enthalpy of formation ΔH(eV/unit cell) and Goldschmidt's tolerance factor (TF) with PBEsol-GGA at 0 GPa.

Parameter	$MgZrO_3$
a_0(Å)	4.08
Other Theoretical	4.13[a]
B_0(GPa)	168.90
ΔH (eV/unit cell)	-2.94
Other theoretical	-2.86[a]
TF	0.98

Ref. [23].

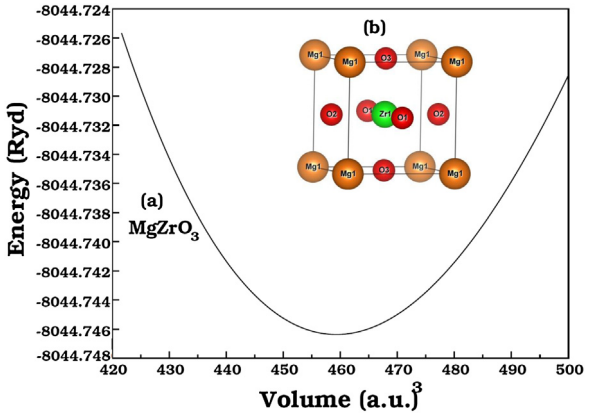

Fig. 1. (a) Energy *vs.* volume plots using PBEsol-GGA and (b) the optimized cubic structure using Xcrysden Software for $MgZrO_3$.

The cubic structure of $MgZrO_3$ with space group Pm-3 m (221) has been optimized to relax the structure as presented in Fig. 1(a, b). The Figure 1(a) shows the optimized energy verse volume plot from which ground state parameters like lattice constant and bulk modulus are calculated by using the Murnaghan equation of states. The calculated parameters are presented in Table 1 that has a close agreement with the other theoretical reports. Moreover, in cubic oxide structure, the doped Zr atom is trapped in the central position of an octahedron of O atoms and tetrahedron of Mg atoms as shown in Fig. 1(b). Further to elucidate the electronic behavior, the calculated electronic band structures at variant pressure up to 25 GPa have been shown in the Fig. 2. It is clear from the Fig. 2, the valence band maxima and conduction band minima lie at the M and Γ symmetry points. We have applied pressure to the structure by shifting the electronic states at same wave vector in the region of first Brillion zone. Therefore, the E_g(Γ-M) and E_g(Γ-Γ) coincide with each other at 25 GPa that reveal transformation of the indirect to direct band gap. The conversion to direct band reduces the phonon heating effect when light falls on the studied oxide and enhance the device life. The insertion of pressure shifts the E_g(Γ-M) to E_g(Γ-Γ) that minimizes the phonon energy. According to relation $hf = hf_0 + h\upsilon$, the hf is the energy of the incident phonons, hf_0 is the direct band gap energy to move the electrons from valence band to the conduction band and $h\upsilon$ is phonon translation energy which

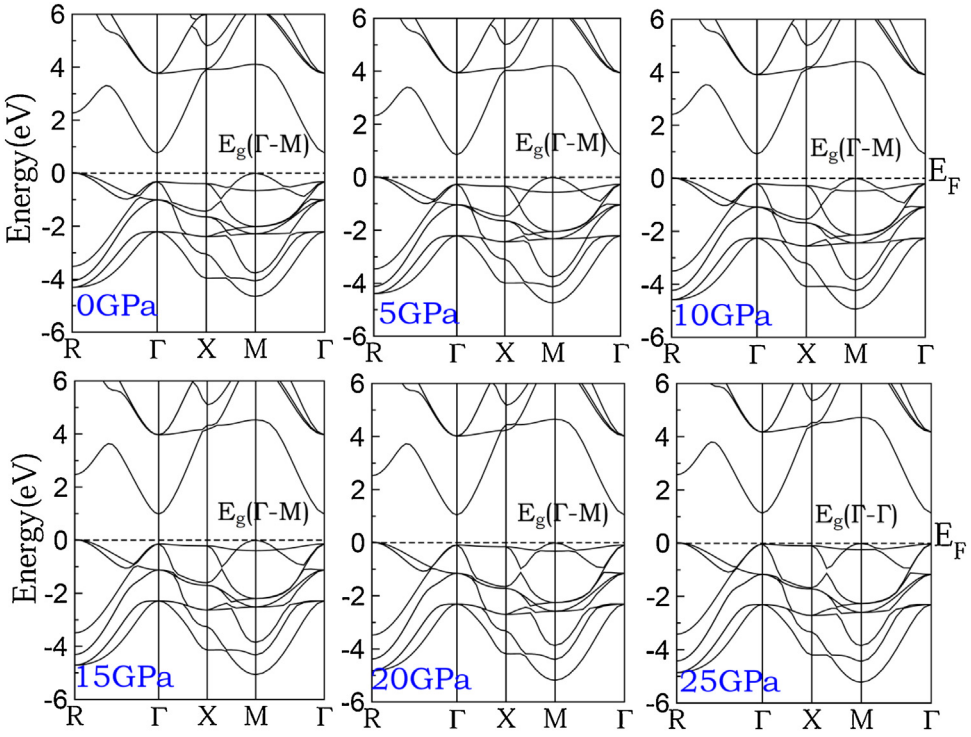

Fig. 2. The calculated band structures of $MgZrO_3$ under the application of applied pressure (0, 5, 10, 15, 20 and 25 GPa).

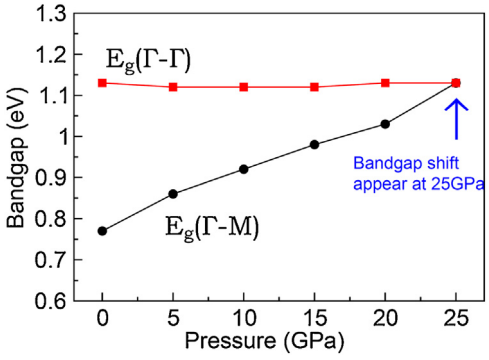

Fig. 3. The pressure-induced variation in the energy band gap of $MgZrO_3$ along high symmetry Γ-X and X-X directions.

becomes zero in direct band gap semiconductors (hf = hf_0=Eg). The phonons in indirect band gap semiconductors create heating effect that reduces the device reliability. It is also clear from the Fig. 3 and Table 2, with the inversion of pressure, the band gap increases that shifts the infrared red region to visible and make the studied oxide potential materials for optoelectronic applications.

3.2. Optical properties

The decreasing of energy production and increasing consumption rate urges the scientific community to search the more ways to meets the energy deficiency. The conversion of light into electrical energy is the best technology that can fulfill the energy needs. This conversion depends upon the band gap, electron-photon interaction inside the studied materials transition rate. The transition of electrons has two types; either band to band transition (inter-band transition) or within the band transition (intra-band transition). The intra-band band transition is important in metals and inter-band transitions are important in semiconductors. Moreover, the band gap should be direct for optoelectronic devices to avoid the phonons that create heating heat and reduce the device efficiency [24–27]. Therefore, for best solar cell and optoelectronic applications the materials have inter-band transitions, direct band gap and threshold frequency allow absorbing the visible light. We have applied pressure 25 GPa to tune the band of the $MgZrO_3$ and calculated optical properties in terms of dielectric constant and refraction are presented in the Fig. 4 (a–d). The real part of the complex dielectric constant $\varepsilon_1(\omega)$ describes the scattering of light energy into to constituent wave lengths at resonance frequency and alignment of planes in which the light is polarized while imaginary part of the dielectric constant $\varepsilon_2(\omega)$ tells how much light

Table 2
The calculated indirect band gap E_g(eV), optical parameters and room temperature thermoelectric coefficients of $MgZrO_3$ perovskite at different pressure.

Pressure in GPa	E_g(eV)	$e_1(0)$	n(0)	s(×10^{14}W/mKs)	κ(×10^{14}W/mKs)	S(μV/K)	PF	ZT
0	0.77,0.62[a]	5.08	2.25	11.57	1.737	182.45	3.85	0.66
5	0.86	4.96	2.23	10.46	1.63	190.48	3.94	0.68
10	0.92	4.92	2.22	12.51	1.94	184.87	4.47	0.64
15	0.98	4.87	2.20	16.08	2.64	190.74	6.14	0.65
20	1.03	4.82	2.19	28.00	3.82	161.30	7.65	0.56
25	1.33	4.68	2.16	50.11	5.85	122.98	8.10	0.39

Ref. [23].

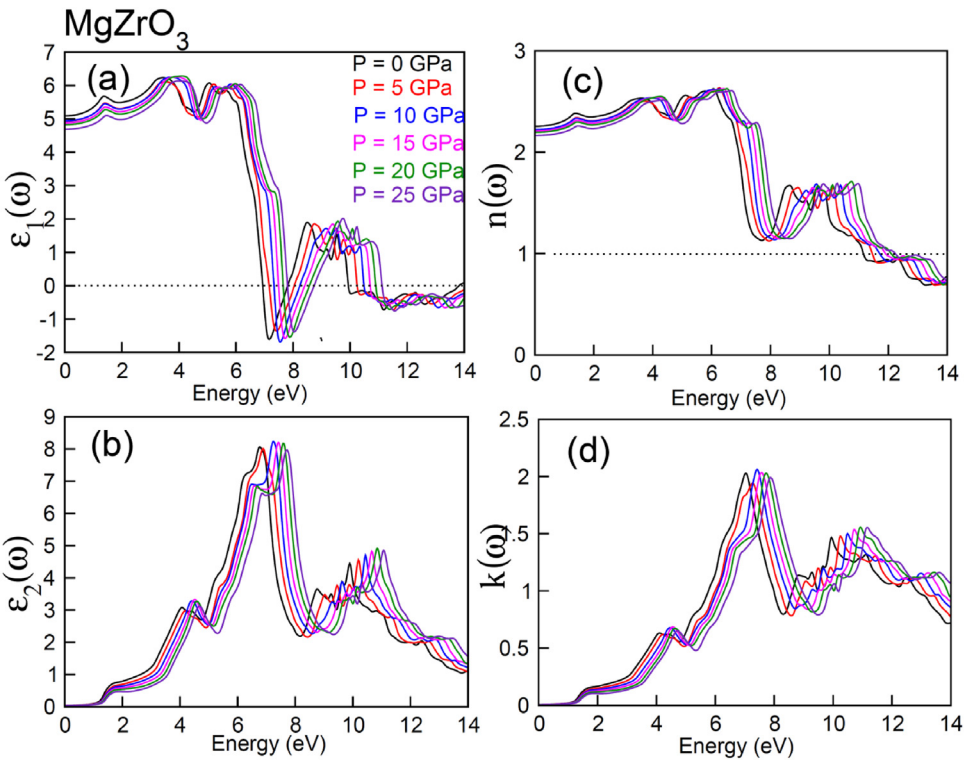

Fig. 4. Calculated (a) real part ε_1 (ω), (b) imaginary part ε_2 (ω) of dielectric constant, refractive index $n(\omega)$ and (d) extension coefficient $k(\omega)$ of $MgZrO_3$ at pressure equal to 0, 5, 10, 15, 20 and 25 GPa.

energy has been absorbed by the material. The $\varepsilon_1(\omega)$ and $\varepsilon_2(\omega)$ are related through Kramer-Korong relation as described in the Ref [28]. The $\varepsilon_1(\omega)$ increases from zero frequency limit and reaches to peak value (5.9) at 4 eV, then decreases to the minimum value (-1.5) at 7.5 eV, due to a little change in frequency from resonating limit. The negative value of $\varepsilon_1(\omega)$ in the regions 6.7 eV to 9 eVand 10 eV to 14 eV shows the metallic behavior because of zero absorption of light in this region. The insertion of pressure changes the states to high symmetry points due to which the zero-frequency value of $\varepsilon_1(0)$ reduces and peak shifted to the high energy region as shown the Fig. 4(a). Moreover, the zero-frequency value of the $\varepsilon_1(0)$ is inversely related to the band gap of the studied materials according to Penn's model [29] as shown in the band structure plots in Fig. 2.

When light falls on the material surface, the high energy radiations are absorbed in the upper surface of the material and low energy photons are penetrate in the material according to wavelength. The $\varepsilon_2(\omega)$ shows how much light absorbed by the material before it transmits through the material. The attenuation of the light by material for the fixed frequency at variant pressure is presented in the Fig. 4(b). The photons are only absorbed when they have energy greater than the band gap of the studied material. Therefore, zero frequency limit of the $\varepsilon_2(\omega)$ shows the optical band gap which is consistent with the band gap reported from band structure plot that shows the reliability of our theoretical calculations. It is clear from the Fig. 4(b); the absorption of light becomes maximum in an ultraviolet region where the dispersion of light has a negative slope. This type of ceramic materials is important for sterilizing surgical tools and optoelectronic device fabrication. The implementation of pressure moves the peaks slightly toward higher energy region that reduce the wavelength and blue shift has been taken place. The refractive index n (ω) similar to $\varepsilon_1(\omega)$ disperse the light into its constituent colors and shows the transparency of the studied material [30,31]. The calculated values of refractive index n(ω) at a variant pressure from 0-25 GPa have been presented in the Fig. 4(c). After 11.2 eV the n(ω) has fractional values that show the group velocity of the studied material exceed from the phase velocity according to the relation $V_g(1 - \lambda dn/nd\lambda) = \vartheta_P$. This fact changes the material response from right handed to lift handed that has not been yet discovered. The extinction coefficient k (ω) has been related to $\varepsilon_2(\omega)$ through $2nk$ (ω)= $\varepsilon_2(\omega)$. Therefore, the $k(\omega)$ has replica of $\varepsilon_2(\omega)$ as shown in the Fig. 4(d). Moreover, the ratio of imaginary part of the dielectric constant to extinction coefficient ratio is equivalent to the refractive index of the $MgZrO_3$ that usually 2 to 3 for best optoelectronic material.

3.3. *Thermoelectric properties*

The oxide materials like magnesium zirconia oxide ($MgZrO_3$) are considered potential materials for thermoelectric applications because of these are cost-effective, highly efficient and easy to handle while device fabrication. Thermoelectric devices, generators, refrigerators, thermocouples are of most important in the growing age because wasted heat energy is converted into useful electrical energy. The thermoelectric properties of semiconductor materials depend upon the band gap and type of carriers available for conduction in the materials [32–36]. We have elaborated the thermoelectric behavior of the $MgZrO_3$ by calculating the electrical conductivity (σ), thermal conductivity (κ) and See-beck coefficient ($S = \Delta V/\Delta T$) by using the BoltzTraP code [37]. The thermal efficiency without and with thermal conductivity has been analyzed by power factor ($P = \sigma S^2$) and thermal efficiency ($ZT = \sigma S^2/\kappa\ T$) [38]. The calculated values of these prescribed parameters in the temperature range 0-900 K and chemical potential -4 to +4 are shown in the Figs. 5–8. The electrical conductivity measures the number of carriers available for conduction mechanism. The values

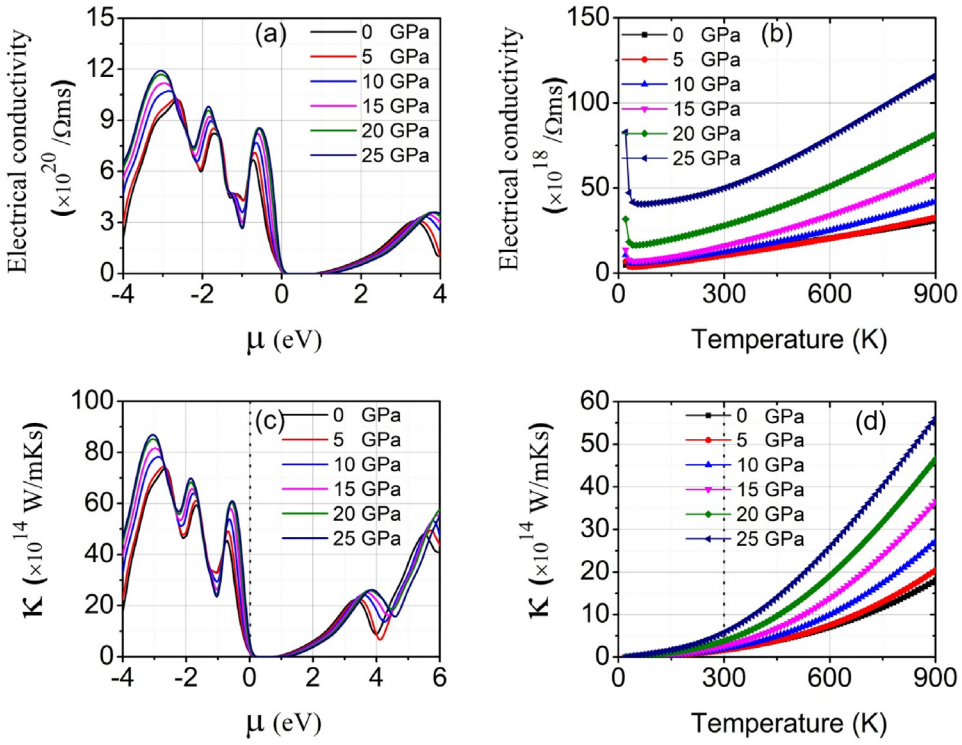

Fig. 5. Calculated electrical and thermal conductivieties of $MgZrO_3$ against (a, c) chemical potential and (b, d) temperature at pressure equal to 0, 5, 10, 15, 20 and 25 GPa.

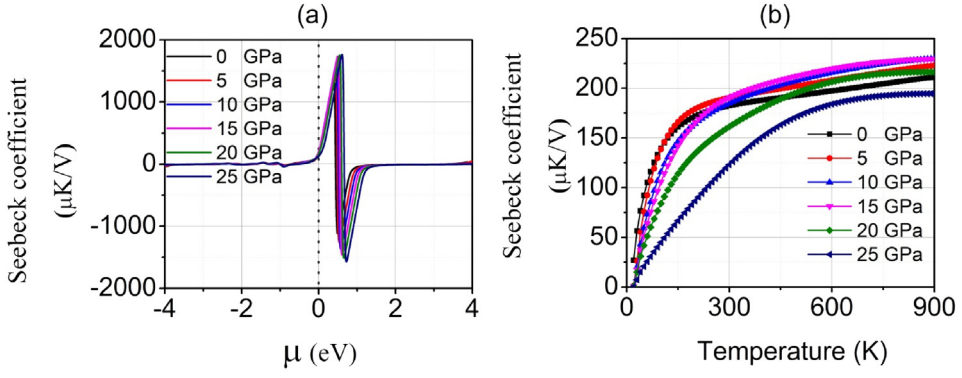

Fig. 6. Calculated seebeck coefficient of $MgZrO_3$ against (a) chemical potential and (b) temperature at pressure equal to 0, 5, 10, 15, 20 and 25 GPa.

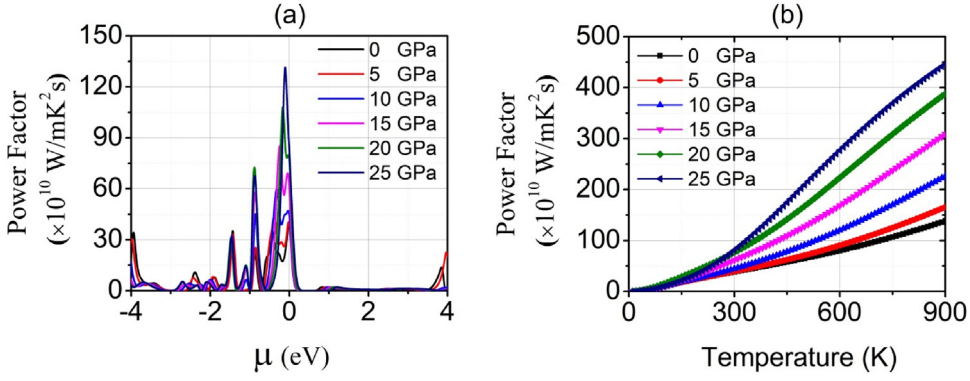

Fig. 7. Calculated power factor of $MgZrO_3$ against (a) chemical potential and (b) temperature at pressure equal to 0, 5, 10, 15, 20 and 25 GPa.

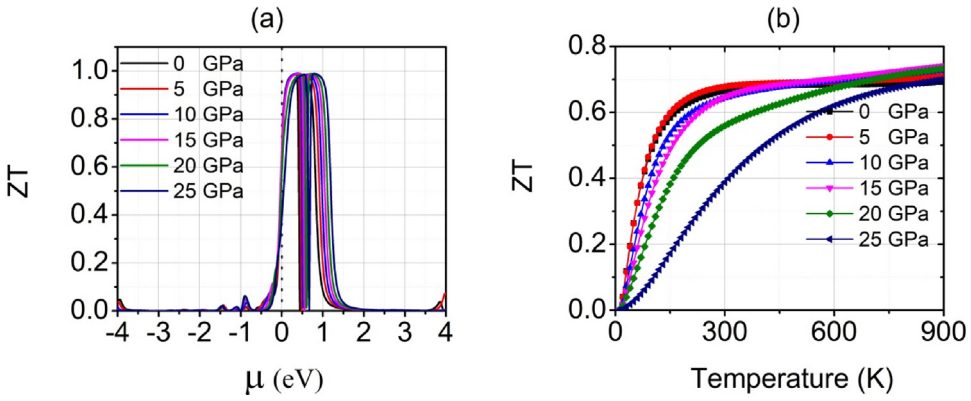

Fig. 8. Calculated ZT values of $MgZrO_3$ against (a) chemical potential and (b) temperature at pressure equal to 0, 5, 10, 15, 20 and 25 GPa.

of electrical conductivity should be high for efficient thermoelectric devices to reduce the Joule heating effect in semiconductors [39]. The electrical conductivity verse chemical potential (μ) plot has been presented in the Fig. 5(a) in which Fermi level adjusted at zero potential. Basically, the chemical potential is energy required for the incoming electron when one electron has been added or removed to the system. The negative value of chemical potential shows the removal of an electron and positive value shows the addition of an electron. The deficiency of electrons corresponds to p-type character and excess of electrons n-type character. The value of electrical conductivity increases from Fermi level in the valence band to 8×10^{20} /Ωms (-0.8 eV) for first removal, 10×10^{20} /Ωms (−2 eV) for second removal and 12×10^{20} /Ωms (−3 eV) for the third removal of electrons. The hole concentration increases as the value of chemical potential become more negative because of the higher order of removal of electrons from the grip of the nucleus on remaining electrons increases. On the other hand, for the n-typeregion, the value of electrical conductivity only reaches to 3×10^{20} /Ωms (4 eV). Therefore, it is clear that the studied material is p-type semiconductor. It is also seen from the Fig. 5(a), by applying pressure the electrical conductivity increases because the band gap shifted from indirect to direct. Furthermore, the increasing value of electrical conductivity with temperature at variant pressure has been shown in Fig. 5(b) that shows the electrical conductivity increases linearly with the rise of temperature because carriers gain kinetic energy and bond breaking take place that produces more carriers for conduction. The decreasing slope of the curves clearly shows the decrease of electrical conductivity may be due to increases the resistance to the rise of pressure.

The thermal conductivity is the ratio of heat efflux to temperature change per unit length whose value can be calculated Fourier's law $q = -k\nabla_x(T)$, where q is the heat efflux, $\nabla_x(T)$ is the temperature gradient and k is the coefficient of thermal conductivity. In semiconductors, both the electrons k_e and phonons k_ℓ are responsible for conduction mechanism [40]. In metals, the intraband transitions are taking place and phonons vibrations cannot be ignored while in semiconductors inter-band transitions are dominant. Therefore, to make the calculation convenient, we have only discussed the electronic contribution to thermal conductivity. It is clear from the Fig. 5(c), the thermal conductivity has a similar trend as electrical conductivity. Its value for first, second and third mode increases as 60×10^{14}W/mKs (-0.8 eV), 70×10^{14}W/mKs (−2 eV) and 86×10^{14}W/mKs (−3 eV) respectively. The thermal conductivity increases as the temperature because at a high temperature more carriers are available for conduction. The effect of pressure creates a resistive effect as explained above and increases the thermal conductivity as seen in the Fig. 5(d). Moreover, the Wiedemann-Franz constant ratio $LT = k/\sigma$ is very low for the studied materials [41] of the order of 10^{-6} that confirms the importance of these materials for device fabrication.

The potential gradient/seebeck coefficient (S = ΔV/ΔT) also measure the flow carriers from high-temperature region to the low-temperature region whose graphical trends versus chemical potential and temperature are presented in the Fig. 6(a) and Fig. 6(b). The potential gradient in the p-type region is zero while in the n-type region its value fluctuates from -1500μV/k to 1800 μV/K at the chemical potential 0.8 eV. This sharp variation of potential shows the electrons are minority charge carriers in the conduction band. To see the temperature effect on potential gradient at variant pressure, the seebeck coefficient has been plotted in the temperature range 0-900 K as shown in Fig. 6(b). Its value increases sharply up to 200μV/K then becomes almost constant. It is also clear the value of seebeck coefficient first increases with pressure up to 15 GPa and then decreases up to 25 GPa at 900 K due to a different value of potential gradient.

Power factor is the product of electrical conductivity and square of the potential gradient. It is clear from the Fig. 7(a) and Fig. 7(b), the major contributor to power factor is the electrical conductivity because electrical has high values in the valence band edge while seebeck coefficient has sharp variation in the conduction. The cooperative effect of these two parameters shifts the power factor at and within the valence band edge that shows majority charge carriers are holes in the p-type region. Moreover, the value of power factor increases linearly with increasing the temperature. The effect of pressure increases the slopes of the curves because the electrical conductivity has a high slope with increasing pressure.

The thermoelectric efficiency can be analyzed from the figure of merit by including the thermal contribution by using the following mathematical relation $ZT = \sigma S^2/\kappa T$ [38]. The calculated values of the figure of merit plot for $MgZrO_3$ at variant pressure against chemical potential and increasing temperature have been plotted in the Fig. 8(a) and Fig. 8(b). Its peak value reaches to 1 that shows the studied materials are best thermoelectric materials. Moreover, with increasing temperature, its value increases sharply up to the 200 K and then becomes constant. The increasing pressure decreases the slopes of the curves at low temperature while it becomes constant at high temperature. The values of thermoelectric parameters at room temperature are presented in Table 2, shows the electrical conductivity, thermal conductivity and Seebeck coefficient increases with increasing pressure up to 25 GPa. This increases the power factor while decreases the figure of merit value. It means the thermal effect reduce the efficiency at high temperature. Moreover,

the efficiency and band gap of the studied material have an inverse relation.

The whole analysis of studied material shows the studied material has maximum absorption in the ultraviolet region and direct band gap at 25 GPa that increases their importance for solar cell and optoelectronic applications. On the other hand, the thermal efficiency is high at ambient pressure and decreases with increasing pressure. Therefore, at high pressure, we can prefer the studied materials for optical applications and at ambient pressure for thermoelectric applications.

4. Conclusions

In the present article, electronic, optical and thermoelectric properties of $MgZrO_3$ oxide has been explored by using modified Becke-Johnson potential as developed in the FP-LAPW + lo method based WIEN2k code. The negative value of formation energy and tolerance factor equivalent to unity confirms the thermodynamic and structural stability of $MgZrO_3$. The external pressure of magnitude 25 GPa has been found to tune nature of the band gap from indirect to direct band gap. The high value of absorption coefficient in UV-region makes the studied materials important for optoelectronic applications. Moreover, electrical and thermal conductivities are directly related with pressure and temperature that minimize the Wiedemann-Franz constant. Furthermore, the power factor increases with increasing pressure while the figure of merit decreases. Therefore, the insertion of pressure enhances the band gap and decreases the thermal efficiency. Finally, it is concluded that at ambient pressure thermal efficiency is high and at 25 GPa the material is optically active.

Acknowledgment

The author (Bakhtiar Ul Haq) would like to express his gratitude to Research Center of Advanced Materials -King Khalid University, Saudi Arabia for support. The author A. Laref acknowledges the financial support by a grant from the "Research Center of the Female Scientific and Medical Colleges", Deanship of Scientific Research, King Saud University.

References

[1] D. Kuzum, S. Yu, H.-S. Philip Wong, Synaptic electronics: materials, devices and applications, Nanotechnology 24 (2013), 382001.
[2] H. Przybylińska, G. Springholz, R.T. Lechner, M. Hassan, M. Wegscheider, W. Jantsch, G. Bauer, Magnetic-Field-Induced Ferroelectric Polarization Reversal in the Multiferroic $Ge_{1-x}Mn_xTe$ Semiconductor, Phys. Rev. Lett. 112 (4) (2014), 047202.
[3] R.T. Lechner, G. Springholz, M. Hassan, H. Groiss, R. Kirchschlager, J. Stangl, N. Hrauda, G. Bauer, Phase separation and exchange biasing in the ferromagnetic IV-VI semiconductor $Ge_{1-x}Mn_xTe$, Appl. Phys. Lett. 97 (2010), 023101.
[4] M. Hassan, G. Springholz, R.T. Lechner, H. Groiss, R. Kirchschlager, G. Bauer, Molecular beam epitaxy of single phase GeMnTe with high ferromagnetic transition temperature, J. Cry. Growth 323 (1) (2011) 363–367.
[5] S. Jiang, Y. Fang, R. Li, H. Xiao, J. Crowley, C. Wang, T.J. White, W.A. Goddard III, Z. Wang, T. Baikie, J. Fang, Pressure-Dependent Polymorphism and Band-Gap Tuning of Methylammonium Lead Iodide Perovskite, Angew. Chem. Int. Ed. 55 (2016) 6540.
[6] N.A. Noor, M. Hassan, M. Rashid, S.M. Alay-e-Abbas, A. Laref, Systematic study of elastic, electronic, optical and thermoelectric properties of cubic $BiBO_3$ and $BiAlO_3$ compounds at different pressure by using abinitio calculations, Materials Research Bulletin 9 (2018) 436–443.
[7] H.T. Hauge, M.A. Verheijen, S. Conesa-Boj, T. Etzelstorfer, M. Watzinger, D. Kriegner, I. Zardo, C. Fasolato, F. Capitani, P. Postorino, S. Kölling, A. Li, S. Assali, J. Stangl, E.P.A.M. Bakkers, Hexagonal silicon realized, Nano Lett. 15 (2015) 5855.
[8] J.S. Williams, B. Haberl, S. Deshmukh, B.C. Johnson, B.D. Malone, M.L. Cohen, J.E. Brad, Hexagonal germanium formed via a pressure-induced phase transformation of amorphous germanium under controlled nanoindentation, Phys. Status Solidi RRL 7 (2013) 355.
[9] P. Bogustawski, Stability of epitaxial $Ga_{0.5}In_{0.5}P$ ordered alloys: effects of dimensionality, Semi. Sci. Technol. 6 (1991) 953.
[10] A.Ş. Demirkıran, E. Avcı, Evaluation of functionally gradient coatings produced by plasma-spray technique, Surface and Coatings Technology 116–119 (1999) 292–295.
[11] A. Kawashima, K. Matsubara, K. Honda, Development of heterogeneous base catalysts for biodiesel production, Bioresource Technology 99 (2008) 3439–3443.
[12] Y. Zhang, L. Li, W. Bai, B. Shen, J. Zhai, B. Li, Effect of CaZrO 3 on phase structure and electrical properties of KNN-based lead-free ceramics, RSC Adv. 5 (2015) 19647–19651.
[13] B.J. Kennedy, C.J. Howard, B.C. Chakooumakos, High-temperature phase transitions in $SrZrO_3$, Phys. Rev. B 59 (1999) 4023.
[14] S. Yamanaka, H. Fujikane, T. Hamaguchi, H. Muta, T. Oyama, T. Matsuda, S. Kobayashi, K. Kurosaki, Thermophysical properties of $BaZrO_3$ and $BaCeO_3$, J. Alloys Compd. 359 (2003) 109.
[15] P. Blaha, K. Schwarz, G.K.H. Madsen, D. Kvasnicka, J. Luitz, WIEN2K, An augmented plane wave + local orbitals program for calculating crystal properties, Karlheinz Schwarz, Techn. Universität Wien, Austria), 2001.
[16] Walter Kohn, Lu Jeu Sham, Self-Consistent Equations Including Exchange and Correlation Effects, Physical Review. 140 (1965) A1133–A1138.
[17] J.P. Perdew, A. Ruzsinszky, G.I. Csonka, O.A. Vydrov, G.E. Scuseria, L.A. Constantin, X. Zhou, K. Burke, Restoring the density-gradient expansion for exchange in solids and surfaces, Phys. Rev. Lett. 100 (2008), 136406.
[18] H.J. Monkhorst, J.D. Pack, Special points for Brillouin-zone integrations, Phys. Rev. B 13 (1976) 5188.
[19] G.K.H. Madsen, D.J. Singh, TraP Boltz, A code for calculating band-structure dependent quantities, Comp. Phys. Comm. 175 (2006) 67.
[20] Masood Yousaf, F. Inam, R. Khenata, G. Murtazad, A.R.M. Isa, M.A. Saeed, Prediction study of structural, electronic and optical properties of XIn2S4 (X = Hg, Zn) thiospinels under pressure effect, J. Alloys Compnds 589 (2014) 353–363.
[21] B. Sabir, G. Murtaza, Q. Mahmood, R. Ahmad, K.C. Bhamu, First principles investigations of electronics, magnetic, and thermoelectric properties of rare earth based $PrYO_3$ (Y=Cr, V) perovskites, Current Appl. Phys. 17 (2017) 1539–1546.
[22] J. Young, J.M. Rondinelli, Octahedral Rotation Preferences in Perovskite Iodides and Bromides, Phys. Chem. Lett. 7 (2016) 918–922.
[23] W. Tanveer, M.A. Faridi, N.A. Noor, A. Mahmood, B. Amin, First-principles investigation of structural, elastic, electronic and magnetic properties of $Be_{0.75}Co_{0.25}Y$ (Y=S, Se and Te) compounds, Current Appl. Phys. 15 (2015) 1324.
[24] N.A. Noor, S. Ali, G. Murtaza, M. Sajjad, S.M. Alay-e-Abbas, A. Shaukat, Z.A. Alahmed, A.H. Reshak, Theoretical investigation of band gap and optical properties of ZnO1− xTex alloys (x= 0, 0.25, 0.5, 0.75 and 1), Comp. Mat. Sci. 93 (2014) 151.
[25] D. Moghe, L. Wang, C.J. Traverse, A. Redoute, M. Sponsellerb, P.R. Brown, V. Bulovic, R. Lunt, All vapor-deposited lead-free doped $CsSnBr_3$ planar solar cells, Nano Energy 28 (2016) 469–474.
[26] S. Gupta, T. Bendikov, G. Hodes, D. Cahen, $CsSnBr_3$, A Lead-Free Halide Perovskite for Long-Term Solar Cell Application: Insights on SnF_2 Addition, ACS Energy Lett. 1 (2016) 1028–1033.
[27] M. Rashid, N.A. Noor, B. Sabir, S. Ali, M. Sajjad, Ab-initio study of fundamental properties of ternary $ZnO_{1-x}S_x$ alloys by using special quasi-random structures, Comp. Mater. Sci. 91 (2014) 285–291.
[28] L.C. Tang, Y.C. Chang, J.Y. Huang, C.S. Chang, Ab initio calculated frequency-dependent nonlinear optical properties on $CsGeBr_3$, Proc. of Society of Photo-Optical Instrumentation EngineersSPIE 6294 (2006).
[29] D.R. Penn, Wave-number-dependent dielectric function of semiconductors, Phys. Rev. 128 (1962) 2093.
[30] M. Hassan, A. Shahid, Q. Mahmood, Structural, electronic, optical and thermoelectric investigations of antiperovskites A_3SnO (A = Ca, Sr, Ba) using density functional theory, Solid State Communications 270 (2018) 92–98.
[31] M. Hassan, I. Arshad, Q. Mahmood, Computational study of electronic, optical and thermoelectric properties of X3PbO (X= Ca, Sr, Ba) anti-perovskites, Semicond. Sci. Technol. 32 (2017) 115002.
[32] M. Ullah, G. Murtazaa, Shahid M. Ramay, Asif Mahmood, Structural, electronic, optical and thermoelectric properties of Mg_3X_2 (X= N, P, As, Sb, Bi) compounds, Materials Research Bulletin 91 (2017) 22–30.
[33] K.G. Prasad, Manish K. Niranjan, S. Asthana, Electronic structure, vibrational and thermoelectric properties of $AgTaO_3$: A first-principles study, J. Alloys. Comp. 696 (2017) 1168–1173.
[34] M. Bilal, M. Shafiq Saifullah, B. Khan, H.A.R. Aliabad, S.J. Asadabadi, R. Ahmed, I. Ahmad, Antiperovskite compounds $SbNSr_3$ and $BiNSr_3$: Potential candidates for thermoelectric renewable energy generators, Phys. Lett. A 379 (2015) 206–210.
[35] Z. Mousavi, M.E. Zare, M.S. Niasari, Magnetic and optical properties of zinc chromite nanostructures prepared by microwave method, Trans. Nonferrous Met. Soc. China 25 (2015) 3980–3986.
[36] H. Kim, B. Anasori, Y. Gogotsi, H.N. Alshareef, Thermoelectric Properties of Two-Dimensional Molybdenum-based MXenes, Chem. Mater. 29 (2017) 6472–6479.
[37] L. Yu, W. Kassem, R. Bude, L. Divay, J. Amrit, S. Volz, Thermoelectric property analysis of CsSnX3 materials (X = I, Br, Cl), IEEE Xplore (2016), http://dx.doi.org/10.1109/THERMINIC.2015.7389628.

[38] H.A.R. Aliabad, M. Ghazanfari, I. Ahmad, M.A. Saeed, Ab initio calculations of structural, optical and thermoelectric properties for $CoSb_3$ and ACo_4Sb_{12} (A= La, Tl and Y) compounds, Comp. Mater. Sci. 65 (2012) 509–519.
[39] B. Amin, F. Majid, M.B. Saddique, B.U. Haq, A. Laref, Physical properties of half-metallic $AMnO_3$ (A= Mg, Ca) oxides via ab initio calculations, Comp. Mater. Sci. 146 (2018) 248–254.
[40] S.A. Khandy, D.C. Gupta, Structural, elastic and thermo-electronic properties of paramagnetic perovskite $PbTaO_3$, RSC Adv. 6 (2016) 48009.
[41] J.E. Saal, S. Kirklin, M. Aykol, B. Meredig, C. Wolverton, Materials design and discovery with high-throughput density functional theory: the open quantum materials database (OQMD), JOM 65 (2013) 1501.